L. Pinelli, M. Marconcini, R. Pacciani, A. Notaristefano, P. Gaetani (2023) *The Effects of Swirling Flows in Entropy Wave Convection Through High-Pressure Turbine Stage*, ASME Journal of Turbomachinery, Vol. 145, 031004, doi: 10.1115/1.4055613

The final publication is available at https://doi.org/10.1115/1.4055613

The Effects of Swirling Flows in Entropy Wave Convection through High Pressure Turbine Stage

Lorenzo Pinelli*
Michele Marconcini
Roberto Pacciani
Department of Industrial Engineering
University of Florence
Via S. Marta 3, 50139 Florence, Italy
lorenzo.pinelli@unifi.it

Andrea Notaristefano,
Paolo Gaetani
Energy Department
Politecnico di Milano
Via Lambruschini 4, 20158 Milano, Italy
andrea.notaristefano@polimi.it

ABSTRACT

First stages of aeronautical high-pressure turbines are subjected to significant inlet distortions generated by the combustor system. These disturbances are characterized by velocity and temperature fluctuations convected downstream by the flow. Such perturbations are commonly defined as vorticity and entropy waves and interact with the turbine stages affecting the aerodynamic performance, the heat exchange and generating indirect noise. Moreover, the presence of a swirling flow highly influences the convection and migration of the entropy wave, thus its interaction with the stage. The paper presents an in-depth study of the impact of the swirling flows on the entropy wave evolution by means of experimental campaigns and numerical simulations. Experimental campaigns have been carried out at Politecnico di Milano where a high-pressure turbine rig was equipped with a novel combustor simulator able to generate entropy waves and swirl profiles. Numerical simulations have been performed at the University of Florence by applying time accurate simulation schemes, including incoming disturbances, implemented in the CFD TRAF code. Two

different entropy waves (featuring frequencies of 10 and 110 Hz) injected in a counterclockwise swirling region at midspan have been analyzed at two clocking positions: passage aligned and vane aligned. An excellent agreement is found between experimental acquisitions and numerical results: both show an important reduction of the temperature fluctuations through the stage and highlight the effect of the swirling profile on secondary flows and blade wakes. The extensive comparison reported in the paper validates the numerical approach (based on URANS simulations post-processed by a dedicated filtering technique) which has been further applied to study the impact of swirling flows with an opposite rotation (clockwise). The broad numerical investigation combined with the extensive experimental campaign leads to a deeper understanding of the aerodynamic, thermal, and acoustic implications related to entropy wave evolution in a swirling flow highlighting the interaction phenomena and suggesting how to minimize the impact of entropy waves by comparing the results of the different injection positions and swirling flow directions.

INTRODUCTION

The mutual interaction of combustor-turbine modules in aeronautical engines plays a fundamental role on various design aspects deeply affecting the aerodynamic performance, the combustor stability, the heat exchange, and the noise emission. Modern lean-burn combustion systems produce unsteady heat release in high swirling flow enhancing the velocity and temperature distortions entering the first high pressure turbine stage. The component coupling deserves to be carefully investigated to match the stringent efficiency and pollutant emission limits for greenhouse gas and noise [1–7].

Flow non-uniformities generated by combustors are usually classified in steady temperature distortions, named hot streaks (HS), and pulsating temperature non-uniformities called entropy waves (EW). Both phenomena pose complex problems on the turbine aero-thermodynamics. The latter has also non-negligible implication in the engine noise signature due to the indirect noise generation that occurs in the turbine stage [7]. Indeed, when an entropy wave with no acoustic content is accelerated, indirect noise generation takes place and acoustic waves propagate upstream and downstream the stage. Upstream components may affect the combustor stability, while the downstream ones carry on their propagation along the turbine module up to the exhaust, where they radiate in the far-field increasing the overall noise level emitted by the engine [6]. The presence of swirling flows at the combustor exit complicates the HS and EW evolution within the turbine stage, as the disturbance migration and interaction become highly influenced by the interaction of the swirl component with stage secondary flows. In light of this, an accurate characterization of

swirling entropy wave convection can be considered the ultimate goal of the research on combustor-turbine interaction.

Several investigations on the hot streaks are present in the literature reporting the main effects of steady distortions entering the turbine stage and pointing out the increase of blade surface temperature that depends on the hot flow migration [2, 4], and the generation of additional secondary flows due to temperature gradients [8–10]. Such aspects have already been studied by the authors from the numerical and experimental point of view in [11]. The study of the EW is usually related to the indirect combustion noise (entropy noise) [6, 7, 12] and the numerical and experimental study of this unsteady phenomenon poses additional research issues: the measuring of high frequency temperature fluctuations is still a challenging task [13], while numerical approaches require the use of high-accuracy unsteady solvers and dedicated post-processing tools capable to decompose the overall fluctuations in convected and acoustic perturbations as already shown by the authors [14]. The presence of the swirl motion where the EW evolves, rises the bar of the research activity, and only few works have been published regarding the combined effect on a turbine stage of a swirl profile and hot-streak [15–18]. In this cutting-edge research field, the researchers of the Politecnico di Milano made available the first experimental investigation in the open literature combining both entropy waves and swirling flows with a systematic approach [19, 20]. All these research activities are extremely attractive and the authors decided to take up the challenge to numerically reproduce the experimental evidences.

This work is thus the natural continuation of previous numerical-experimental investigations on entropy wave evolution performed by the authors [14, 21, 22], where the numerical procedure was validated against the experimental data in absence of swirl and the numerical post-processing used to filter the low frequency content related to the EW was presented in detail. In the present work, the additional complexity due to the vortical region was introduced by a modified injector. Two different entropy waves with frequencies of 10 and 110 Hz injected in a counterclockwise swirling region at midspan have been analyzed at two different clocking positions (passage aligned and vane aligned) showing an excellent agreement between numerical results and experimental acquisitions. Then, the impact of a swirling flows with an opposite rotation (clockwise) has been numerically investigated. Finally, entropy noise emissions extracted by the numerical solution are presented. The combination of numerical and experimental evidences increases the understanding of the aerodynamic, thermal, and acoustic implications related to EW evolution in a swirling flow and suggests how to minimize the impact of entropy waves.

In the first part of the paper a brief description of the rig and the entropy wave generator device are

provided together with a summary of the computational setup. Secondly, a wide comparison of EW evolution in the stator and rotor channel at different frequencies, injector positions, and swirl directions is reported pointing out the effect of the swirling entropy wave on secondary flows. Finally, the assessment of the entropy noise generation is reported and discussed in detail.

EXPERIMENTAL SETUP

The description of the experimental setup provided in this paper is shortened for sake of brevity and the interested reader can refer to [20] for further details. Tests have been carried out on the Fluid Machine Laboratory (LFM) high speed test rig, specifically designed for testing turbines and compressors. The meridional view of the test section is shown in Figure 1. First, a centripetal guide vane (IGV in the figure) feeds the axial turbine section and then the flow is straightened by a honeycomb before entering in the stage. The stage is representative of an uncooled HP turbine stage with a leaned stator and a bowed rotor. Stator blade has a lean angle of 12° towards the pressure side. Table 1 summarizes the most relevant information on the geometry and the operating conditions prescribed for the present study. The flow field approaching the turbine stage is uniform with a turbulence intensity of 2.5% and it is perturbed by the Entropy Wave Generator (EWG) extensively described in [19]. In brief, the swirl profile is produced by a swirler generator placed at the injector outlet that acts on both the incoming mainstream air and the injected EW. The latter is generated by an EWG composed by two automotive valves and an air electric heater. The frequency of the automotive valves determines the EW frequency and this set of experiments is carried out at 10 Hz and 110 Hz. These are chosen among the others because 10 Hz allows to preserve the EW magnitude being the mixing process between the cold and hot EW branches less intense; 110 Hz is the

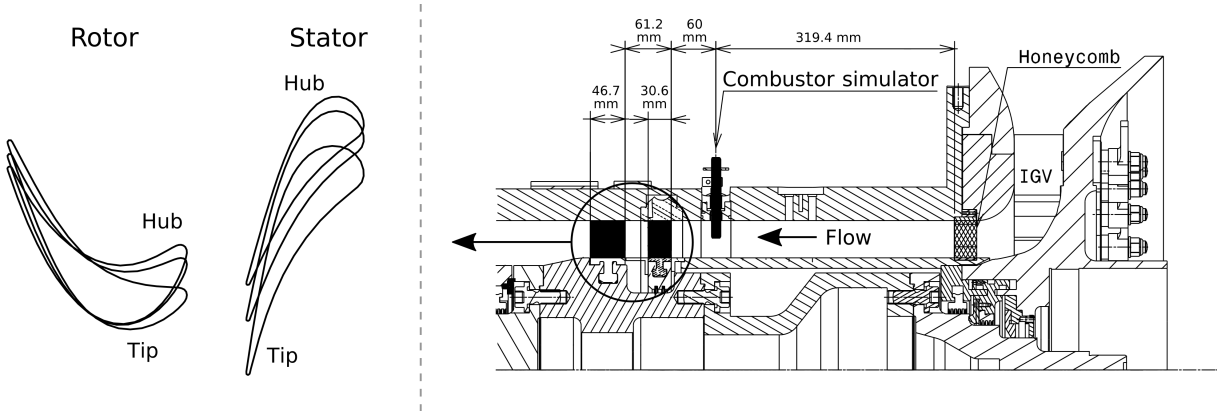

Fig. 1: Turbine meridional view and blade geometry

Table 1: Operative and geometrical stage parameters

Parameters	**Stator**	**Rotor**
Blade Count	22	25
Aspect Ratio	0.83	0.91
Solidity	1.20	1.25
Geometrical blade deflection	75.2°	115.3°
Angular speed [rpm]	-	7000
Outlet Mach number	0.57	0.34
Reynolds number	8.7×10^5	4.4×10^5
Stage Expansion Ratio	1.4	
Inlet Total Temperature T_R [K]	313.15	
EW Injector Count	11	

highest frequency reachable by the used automotive valves and it allows reduced computational time in CFD calculations being a submultiple of the blade passing frequencies. The two flows are then jointed at the head of an injector that forces the EW into the swirler generator.

The combined EW and swirl profile is then injected in the streamwise direction. Temperature is measured with an uncertainty of 0.2 K while pressures with an uncertainty of 0.1% of the transducers range (10 psi and 50 psi ranges are mounted). The combustor simulator can be moved in circumferential direction allowing to inject the disturbance at different clocking positions with respect to the stator vanes. Two injection positions are chosen as the most representative, as shown in Fig. 2: vane aligned (LE in the following) and passage aligned (MP in the following). The first traversing position, upstream of the vane row, is called

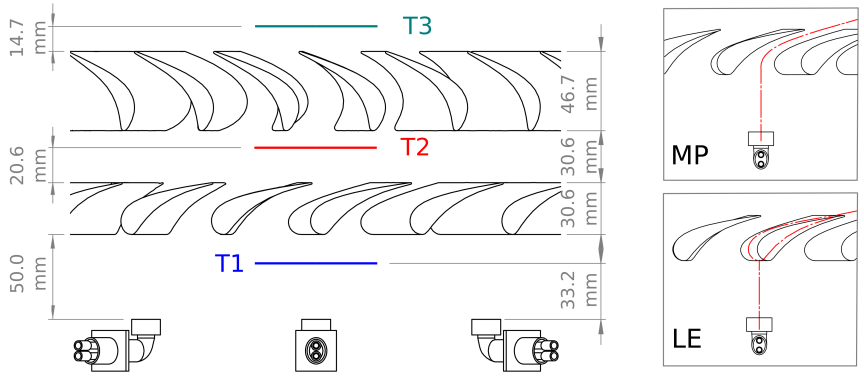

Fig. 2: Measuring planes and injection positions

"T1" where the injected disturbance is characterized. The second position "T2" is located in the vane-rotor spacing at 67% of the vane axial chord downstream of the vane trailing edge; the third position T3 is located downstream of the rotor at 32% of the rotor axial chord. The schematic is reported in Fig. 2. The combustor simulator generates a swirl profile with a swirl number of 0.6 and local swirl angles of $\pm 40°$. The highest EW temperature is 1.26 and 1.18 times the mainstream temperature at 10 and 110 Hz, respectively. Three different turbine inlet conditions are studied: uniform inlet flow called "clean", namely the combustor simulator is removed, and combined injection of a swirl profile and EW at frequencies of "10 Hz" and "110 Hz".

Aerodynamic and temperature probes

Three different probes are traversed to measure flow quantities at the different measuring planes. At positions T1 and T2, by five-hole pressure probes the steady aerodynamic flow field is characterized. The average uncertainties of the two 5-hole probes are calculated using the Monte Carlo method described in [23] that predicts for the probes used at planes T1 and T2 an average extended uncertainty of 0.5° and 0.15° for angles and 50 Pa and 80 Pa for pressure, respectively. Unsteady pressure measurements are carried out at plane T3 through a Fast Response Aerodynamic Pressure Probe (FRAPP), applied as a virtual three-hole probe [24]. FRAPP allows measuring the angle on the blade-to-blade plane with an uncertainty of 0.25° and total/static pressures with an uncertainty of 0.5% of the kinetic head. The probe promptness is up to 100 kHz after dynamic calibration and digital compensation. Phase-averaging techniques are implemented on the blade passing frequencies to reconstruct the time evolution of flow angle, total, and static pressures. Time-resolved temperature measurements are carried out by means of a miniaturized S-type thermocouple with a junction size diameter of 25.4 μm and uncertainty of 0.3 K. Probe promptness is up to 500 Hz after dynamic calibration and digital compensation, thus showing a good reliability in measuring the EW but not to resolve the blade passing frequency. In planes T2 and T3 all probes are traversed circumferentially on a sector of 32.7° that represents the combustor simulator periodicity; at plane T1, probes traversing is carried out just in the zone affected by the disturbance.

NUMERICAL SETUP

The URANS TRAF code has already proven to be capable of simulating the HS (Hot Streak) transport [11] and the EW (Entropy Wave) evolution [14, 22] within the HP stage installed in LFM of the Politecnico di Milano. These previous works extensively validate the computational setup and the dedicated post-processing based on Fourier coefficients by comparing the HS and EW envelopes numerically predicted

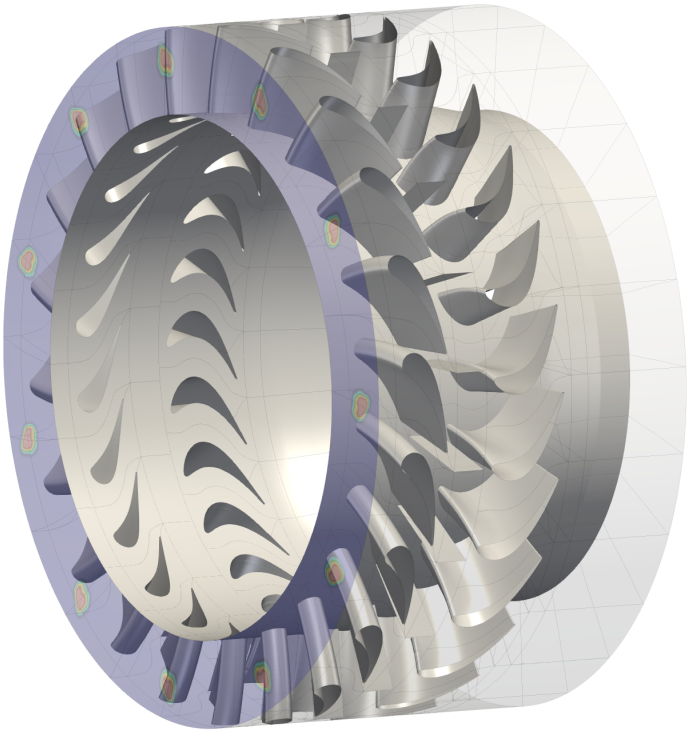

Fig. 3: Full annulus computational domain with inlet spots

within stator and rotor vanes with high-quality experimental acquisitions. The TRAF solver [25] has been developed for more than 30 years at the University of Florence and implements state-of-the-art numerical schemes (e.g., TVD-MUSCL strategy build on the Roe's upwind scheme for convective fluxes [26]) and turbulence models (e.g. $k-\omega$ with $\gamma - Re\theta$ transition model or machine-learned turbulence models [27]) to integrate Reynolds-averaged Navier–Stokes equations with a finite volume formulation on H-type and O-type structured grids. Being a research code, the TRAF solver can be easily customized and integrated into different frameworks [28–30]. For this type of analyses, a time-varying 2D inlet was ad hoc implemented to impose the EW pulsating spots as inlet boundary conditions. Moreover, a run-time Fourier transformation in time of the flow quantities implemented for aeroacoustics studies [31], has been employed to filter the low frequency content associated with the EW spots: the EW amplitude and 3D shape can be extracted by means of a dedicated post-processing tool (fully described in [14]) from the complex Fourier coefficients for comparison purposes.

The computational domain starts from plane T1 and extends far downstream the plane T3 where buffer zones are included to avoid spurious wave reflection during the unsteady runs. Due to the blade count (22/25) that do not allow any domain tangential reduction, the entire stage has been simulated as shown

in Fig. 3. Blade profiles are discretized using an O-type mesh for an accurate boundary layer resolution ($y^+ < 2$ on the wall surfaces), while H-type blocks are used at the inlet, inter-row and outlet regions in order to ensure a sufficient uniform grid density to capture the unsteady phenomena connected to the EW evolution. With this setup, the overall domain consists of 191 blocks for a total number of about 200 Mcells. As in the previous works, the free-stream turbulence intensity imposed at the inlet was locally increased from 2.5% (coming from measurement at the midspan) up to 8.0% in the EW spot region to include the effect of the swirling device. The time discretization was selected to solve up to the second rotor passing frequency (5833 Hz) and leads to a ΔT = 0.014 ms between physical time steps, ensuring the accurate resolution of the EW frequencies that are more than one order of magnitude lower (10 and 110 Hz), and represent a quasi-steady phenomena. For the computation at the lowest EW frequency, the EWF was slightly reduced from 10 Hz to 9.72 Hz so that during a single EW pulsation 12 rotor revolutions occur (rotor revolution frequency is equal to 116.66 Hz) and the overall period (equal to the EW period) becomes T = 102.8 ms. Three EW pulsations were simulated that cover 36 rotor revolutions. For the 110 Hz, the EW frequency was increased to match the rotational frequency of 116.66 Hz: this means that the simulation period reduces to T = 8.5 ms, so that during a single rotor revolution a single EW pulsation happens. For this high frequency analysis, only 4 revolutions (and in turn 4 EW pulsations) were enough to obtain the solution periodicity and the overall simulation time is 9 times lower than 10 Hz case (34.2 ms instead of 308.4 ms). To obtain unsteady results in a reasonable time, the TRAF parallelization [32], achieved by means of a hybrid openMP/MPI code architecture was exploited and all the unsteady runs were computed on a cluster. About 24 CPU hours were needed for the shorter period (8.5 ms) on a Linux cluster of Intel CPU E5-2680 at 2.8 GHz using 150 CPU core.

The above mentioned computational setup was used to perform seven unsteady runs: the first one without any inlet disturbance (the “clean” case), the second pair of computations with the 10 Hz temperature fluctuation and counterclockwise (CCW) steady swirl for the MP and LE positions, and then the 110 Hz

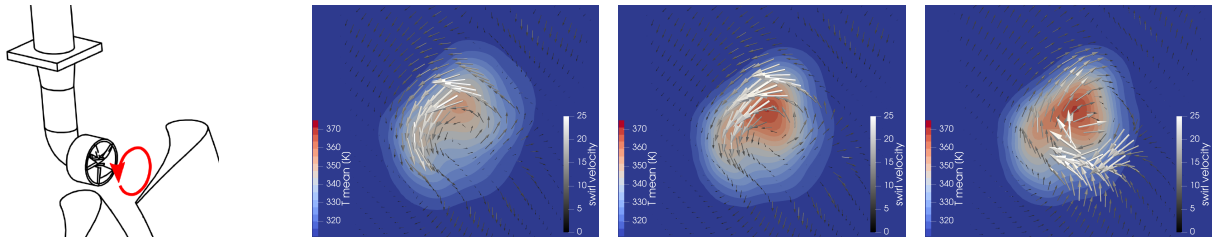

(a) Swirl generator (b) 10 Hz CCW (c) 110 Hz CCW (d) 110 Hz CW

Fig. 4: Entropy spot and swirl velocity imposed at the numerical domain inlet (plane T1)

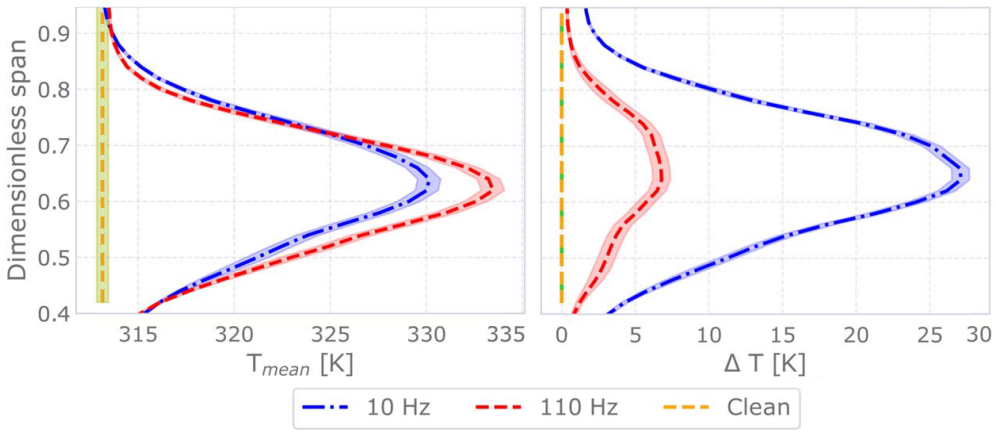

Fig. 5: Measured EW perturbation at the plane T1: mean and peak-to-trough temperature from [20]

temperature pulsation at the MP and LE positions for both counterclockwise (CCW) and clockwise swirl (CW). At the domain inlet, 2D time-varying boundary conditions are applied to reproduce the incoming EW and the swirling flow described in [19]. Figure 4 reports the different injected disturbances imposed at the inlet of the computational domain after a time averaging during a fluctuation period. A schematic view of the swirl device (see Fig. 4a) is also included to clearly define the swirl direction. Figures 4b and 4c show that the incoming disturbances imposed at the inlet, present a similar shape, but a higher value of the mean temperature for the 110 Hz frequency. Such disturbances are injected at mid-span, but due to the swirl flow motion the peak is moved around the 65% of the span. As reported in the experimental study and shown in Fig. 5, the two frequencies have similar mean temperature fields, yet the temperature fluctuation is drastically reduced for the highest frequency because of the high intensity of the mixing process between the hot and cold streams inside the injector [20]. A well-defined swirl vortex with a central re-circulation area is highlighted by the velocity field and the presence of the EW temperature fluctuation increases the mass flow reinforcing the vortex strength. The last disturbance (see Fig. 4d) was artificially generated by inverting the swirl direction to investigate numerically an opposite configuration in terms of the disturbance interaction with the stator secondary flows.

RESULTS AND COMPARISONS

In the following, the numerical results are compared with the experimental acquisitions to highlight the effect of the swirl on the entropy wave propagation throughout the stage. The presented results are directly comparable with the outcomes presented in [14], where the EW spot was injected in an axial flow field for the same injector-stator positions.

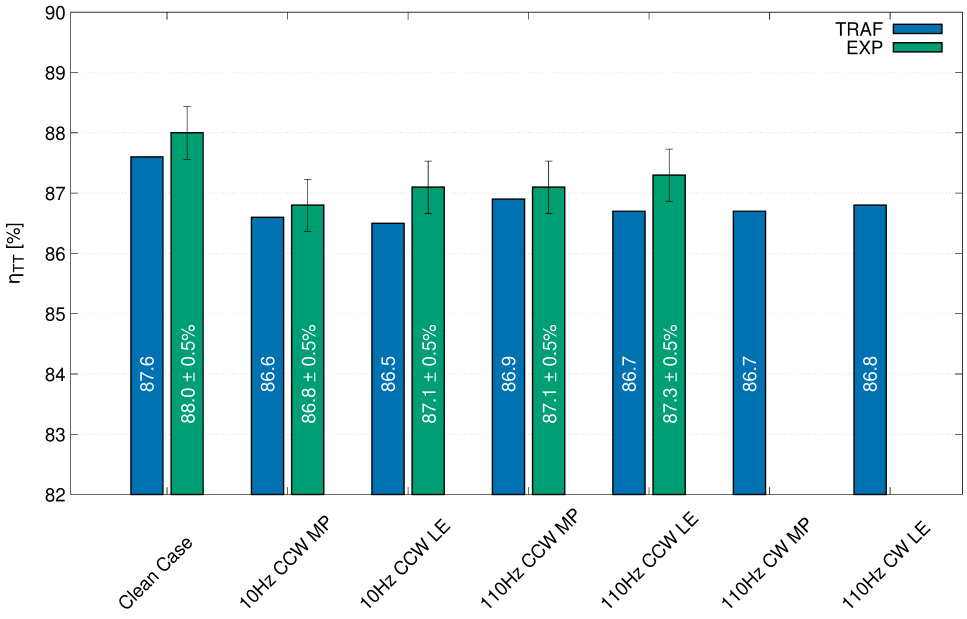

Fig. 6: Stage total-to-total efficiency

Stage efficiency

The stage aerodynamics has been already deeply discussed and compared in previous works by the authors [13, 14], yet a direct comparison of total-to-total stage efficiency is interesting to assess the efficiency loss due to the EW injection. Fig. 6 reports the comparison of the total-to-total efficiency for all the cases. The experimental efficiency is computed as the ratio between the Euler work and total-to-total isentropic enthalpy drop. The Euler work is computed by the mass-averaged on the measuring grid, thus over two stator pitches, of the absolute tangential velocity and the rotational speed at planes T2 and T3. The uncertainty of the efficiency value so calculated is approximately ±0.5% and results comparable with the case-to-case efficiency variation except for the “clean” and “10 Hz CCW LE” cases that show an experimental efficiency variations outside of uncertainty bounds. Furthermore, the experimental values were better corrected to account for rig fluctuations with respect to the results previously shown in [20]. The numerical values are obtained by the mass-averaged of total pressure and total temperature between the same sections. The numerical and experimental values are in agreement, and the slight overestimation in the experimental efficiency is due to the fact that the measurements do not reach exactly the hub and tip section. Overall, both numerical and experimental figures predict that the distortions introduced by the combustor simulator reduce the stage efficiency by about 1%. Despite the relatively high experimental uncertainty with respect to the case variation, experimental and numerical comparisons suggest that the 110

Hz cases have a higher efficiency than 10 Hz and this is consistent with the lower temperature that is found at plane T2 in 110 Hz case than 10 Hz, as it will be shown in the following.

EW evolution in the stator vane

The evolution of the EW spot in the stator channel is mainly driven by the steady swirling flow that differently interacts with the stator secondary flows depending on the injector position. Globally, MP and LE cases exhibit different migrations of the temperature spot in the stator channel despite both disturbances move downward compared to their original position at the plane T1 due to the stator lean geometry. The MP position is subjected to the higher interaction with the nozzle secondary flow, whereas in the LE injection the EW directly impinges on the blade leading edge and is pushed on the suction side by the swirl profile. Such findings are confirmed by the experimental acquisitions [20] and by the present computational results for the CCW swirl as reported in the following for both the analyzed frequencies. Finally, for the 110 Hz case, the numerical results with the CW swirl are presented and compared with CCW swirl.

10 Hz counterclockwise swirl

These investigations, that required the highest computational effort due to the larger disturbance period, show the highest value of temperature fluctuation. Figure 7 shows the iso-contour at ΔT = 12 K within the

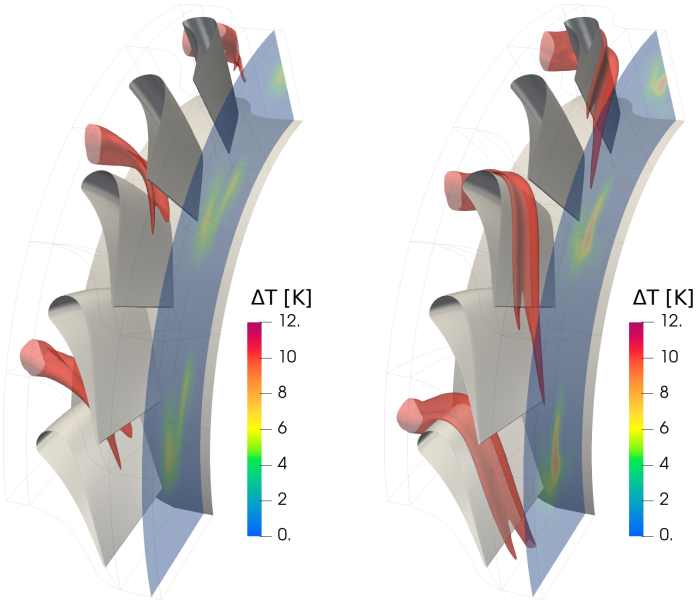

(a) MP injection (b) LE injection

Fig. 7: 10 Hz CCW: spatial evolution of the EW spots within the stator channel

stator vane for both the positions. The MP injection reveals the higher temperature spot diffusion due to the mixing in the high velocity channel region: in fact the iso-contour disappears before reaching the vane exit. Moreover, the swirl generates a distortion on the original circular spot shape that folds the EW disturbance toward the inner channel until assuming a C-shape when extracted at the T2 plane (see Fig. 7a). This disturbance folding is due to the counterclockwise swirl that evolves in a clockwise vorticity field due to the stator lean. In addition to this, previous studies with EW in axial flow revealed an almost circular EW envelope as reported by the authors in [14]. On the other hand, for the LE-aligned case, the spot impacts on the stator LE and is spread on the blade suction side instead of being cut in two branches by the blade as in case of no-swirl (see again [14]). This interaction maintains the spot with a higher core temperature when reaching the plane T2, because the interaction with the secondary flow is prevented. Such conclusions are confirmed when looking at numerical and experimental comparison of the ΔT contours at the plane T2 (see Fig. 8). Despite the well-know lack of diffusion of URANS methods, the EW spot evolution is correctly captured by the simulation, especially for the MP case where the main cause of spot distortion is due to the interaction of the swirl with the secondary flows. For LE case, the agreement of the spot shape is less satisfactory, despite azimuthal and radial, as well as the high temperature value of the EW core, are correctly reproduced. Even in the previous numerical investigations, the LE case turned out to be the most complex to be numerically tackled, as small discrepancies on the spot tangential position can lead to

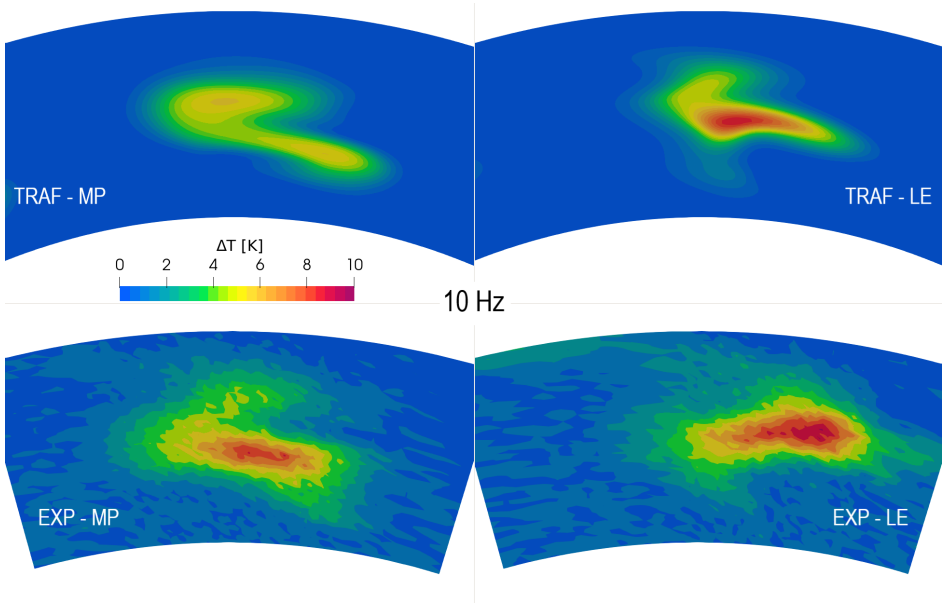

Fig. 8: 10 Hz CCW: num-exp comparison of the amplitude of EW temperature oscillations at the stator exit (plane T2)

different spot propagation. In fact only for this position, the disturbance interacts with the blade boundary layer ending up in the stator wake, thus resulting less affected to the secondary flow effects.

110 Hz counterclockwise Vs. clockwise swirl

The same exercise has been carried out for the 110 Hz cases. Looking at the EW envelope in the stator channel for MP and LE position and CCW swirl (see Fig. 9a and Fig. 9b), a similar shape but with a lower ΔT is found with respect to the 10 Hz cases. The clockwise (CW) swirl results reported in Fig. 9c and Fig. 9d reveal a more compact and less distorted EW footprint due to a different interaction with the secondary flows. This time, the secondary flows do not fold the EW envelope as the adjacent branches of swirl and tip passage vortexes have the same direction and do not vanish as they do in the CCW case where the two branches have different directions as shown in the helicity plots. Again, the ΔT contours at the plane T2 for the CCW swirl are similar to the low frequency case with a reduction to a ΔT_{max} = 2 K. The MP case shows the C-shape disturbance with a remarkable downwash migration, while for the LE case, the spot is mostly extended in the azimuthal direction around midspan. The agreement with the experimental data can be considered satisfactory (see Fig. 10a).

When inverting the swirl direction the EW spot at the plane T2 is quite different. For the MP case, the temperature disturbance preserves a circular shape with only a tangential spreading and locates around

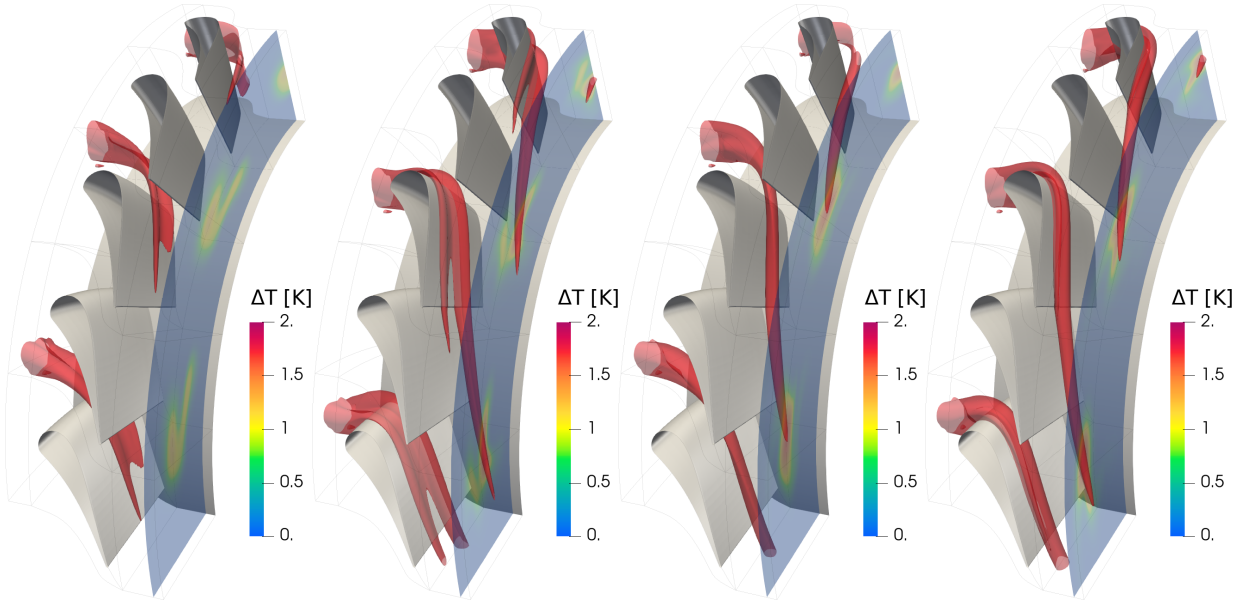

(a) CCW – MP injection (b) CCW – LE injection (c) CW – MP injection (d) CW – LE injection

Fig. 9: 110 Hz: spatial evolution of the EW spots within the stator channel

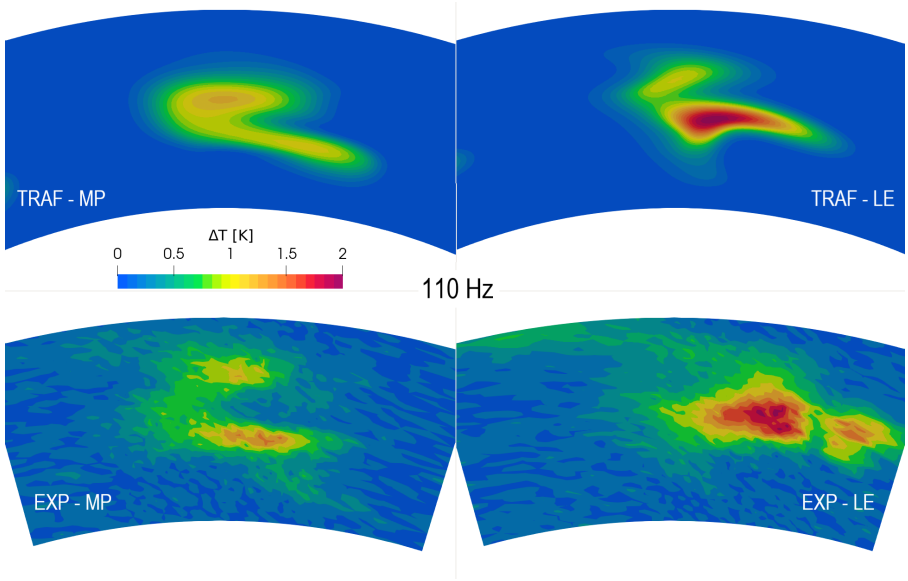

(a) Num-exp comparison for CCW swirling flow

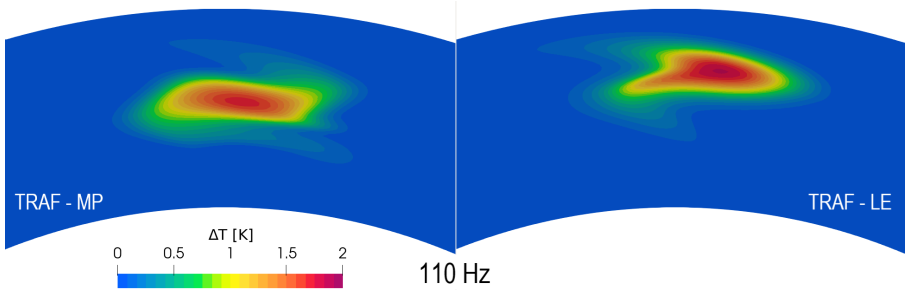

(b) Num-exp comparison for CW swirling flow

Fig. 10: 110 Hz: amplitude of EW temperature oscillations at the stator exit (plane T2)

the mid-span. The spot, resulting from the LE injection, is now located near the tip with the highest ΔT at the spot core. This confirms that the counterclockwise swirl direction promotes the highest diffusion of the EW spot compared with the clockwise swirl condition.

Effect of swirling EW on the stator secondary flows

To highlight the vortical structure at the plane T2 and to find out the trace of the imposed swirling spot, it has been decided to look at the flow helicity defined as the scalar product between flow velocity and vorticity. This provides a useful picture of the streamwise vorticity structures. The preliminary analysis of the “clean” case reported in Fig. 11 allows the description of the main vortical structures serving as a baseline to have a deeper understanding of the cases with EW injections. From the definition, a positive value means a vortical structure that rotates clockwise and vice versa. As can be seen, the stator leaned geometry

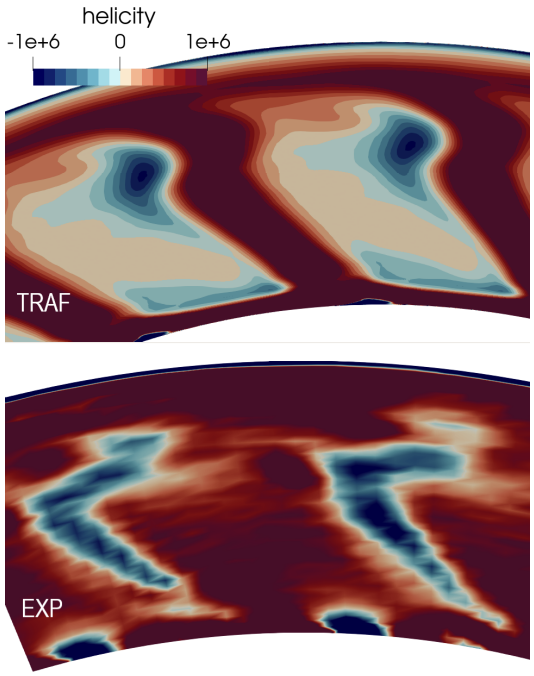

Fig. 11: Clean case: num-exp comparison of the helicity contours at the stator exit (plane T2)

generates a background vorticity with a positive value that is co-rotating with the hub passage vortex and counter-rotating with the tip one. The radial zones with negative value represent the wake vorticity, since the viscous shear between the wake and the positive vorticity (generated by the lean) produces a negative vorticity. Finally, at the hub the negative spot is associated with the hub leakage vortex present in this stator for a specific geometrical feature. Comparing the numerical and experimental contour plots, the main vortical structures associated with the imposed swirl can be found (see the dashed ellipse in Fig. 12a), despite that numerical results show a smaller area of positive vorticity.

Figure 12a presents the numerical-experimental comparison of the vortical structures for the EW at 110 Hz with the CCW swirl; the high temperature spot is also highlighted by the contours marked with “EW”. The EW slightly influences the aerodynamic flow field that is mainly affected by the steady swirl as reported in [19]. In the MP case, the negative swirl vortex (highlighted by the dashed line) remains close to the suction side, and also generates in the above zone a high region of positive vorticity that highly affects the left wake. In the LE case, the counterclockwise vorticity remains on the suction side of near stator, highly modifying the blade wake.

Finally, when looking at the numerical results obtained with the CW swirl a different scenario is found: in the MP case the positive vorticity increases the positive area in the wake region around the blade mid-

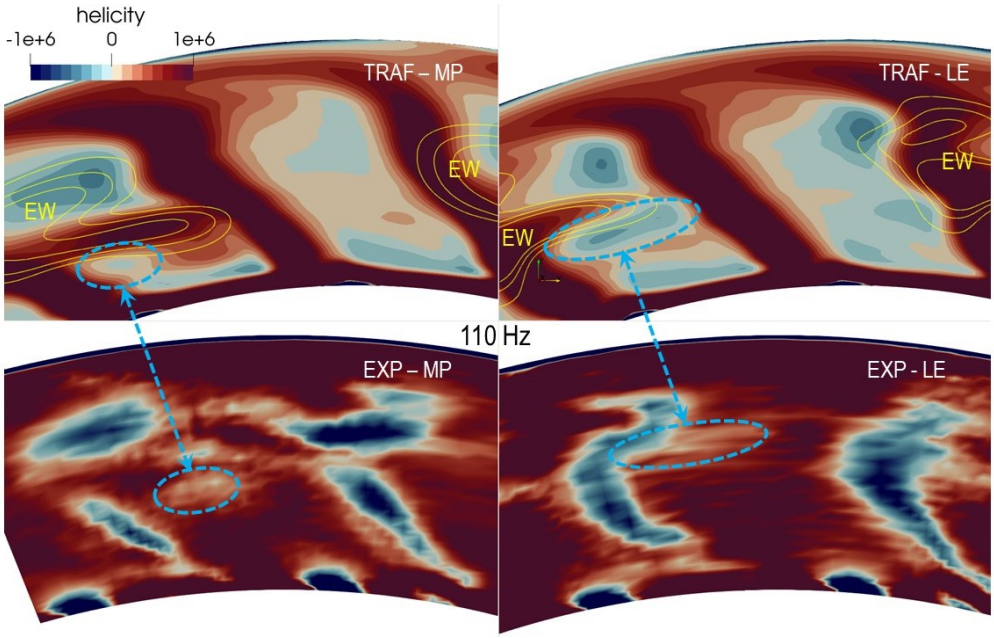

(a) Num-exp comparison for CCW swirling flow

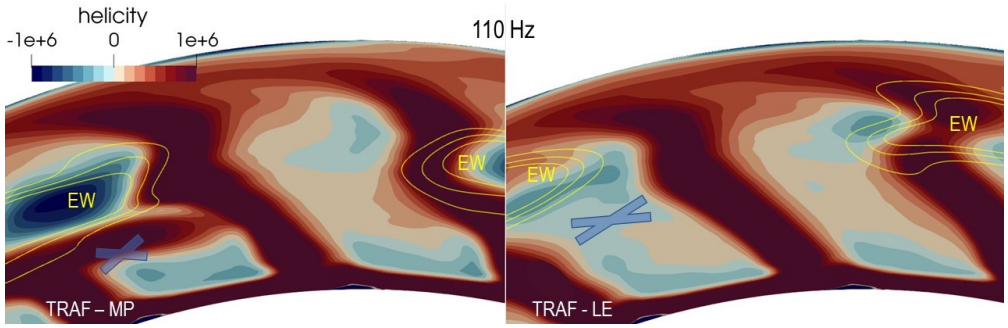

(b) Num-exp comparison for CW swirling flow

Fig. 12: 110 Hz: helicity contours at the stator exit (plane T2)

span and the negative spot disappears (see the cross in Fig. 10b). The LE position shows a vorticity field very similar to the “clean” case with significant modification only in the small area where the EW spot (highlighted with the foreground contours marked with “EW”) is located in tip regions. Again, the negative region detected for the CCW at mid-span is not present anymore (see the location pointed out by the cross).

EW evolution in the rotor vane

The EW evolution in the rotor vane shows a further attenuation of the ΔT and, like in the stator, the two frequencies reveal a similar disturbance evolution despite the different absolute values.

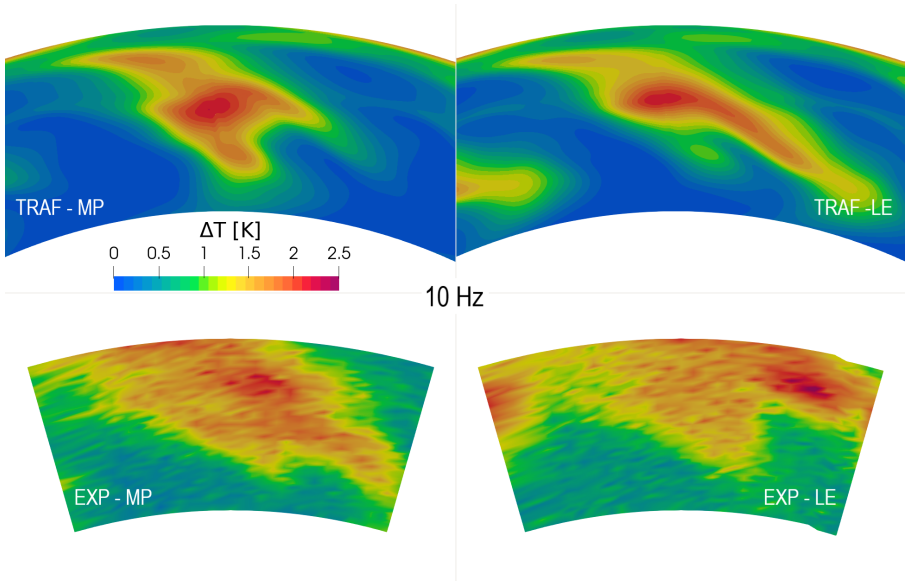

Fig. 13: 10 Hz CCW: num-exp comparison of the amplitude of EW temperature oscillations at the rotor exit (plane T3)

10 Hz counterclockwise

For the 10 Hz cases, only the EW contours at the plane T3 are reported as the channel evolution is similar to the 110 Hz which is presented in the following section in comparison with the clockwise cases. As shown in Fig. 13, there is an excellent agreement between numerical results and experimental data, especially for the MP case. For this case, the EW distortion is distributed radially and impacts the temperature field along all the blade height. For the LE case, the EW is concentrated near the tip region and extends circumferentially: in the numerical prediction the spot is more elongated toward the hub, and this is due to the discrepancies already found at the stator exit for the LE case.

110 Hz counterclockwise Vs. clockwise swirl

Figure 14 depicts the EW path in the rotor channel and the temperature trace on the rotor surface. Due to the rotation, the spot is now spread on all the passages and the high temperature core is located at the mid-span around the middle of the channel for the CCW swirl direction.

The ΔT contours at the plane T3 are similar to the 10 Hz case with the same swirl, but with a very low amplitude hardly detectable by the instrumentation (see Fig. 15). This explains the granular texture of the acquired temperature field that does not allow a direct comparison with the numerical results. Finally, the clockwise swirl direction produces a different temperature field: in this case, the spot remains closer to the tip zone for both the injector positions and is highly elongated in the circumferential direction.

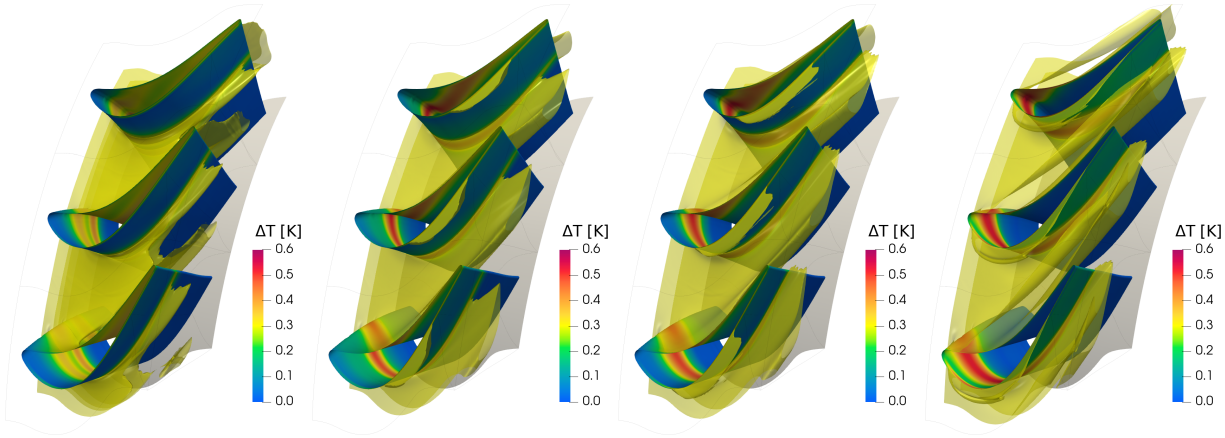

(a) CCW – MP injection (b) CCW – LE injection (c) CW – MP injection (d) CW – LE injection

Fig. 14: 110 Hz: spatial evolution of the EW spots within the rotor channel

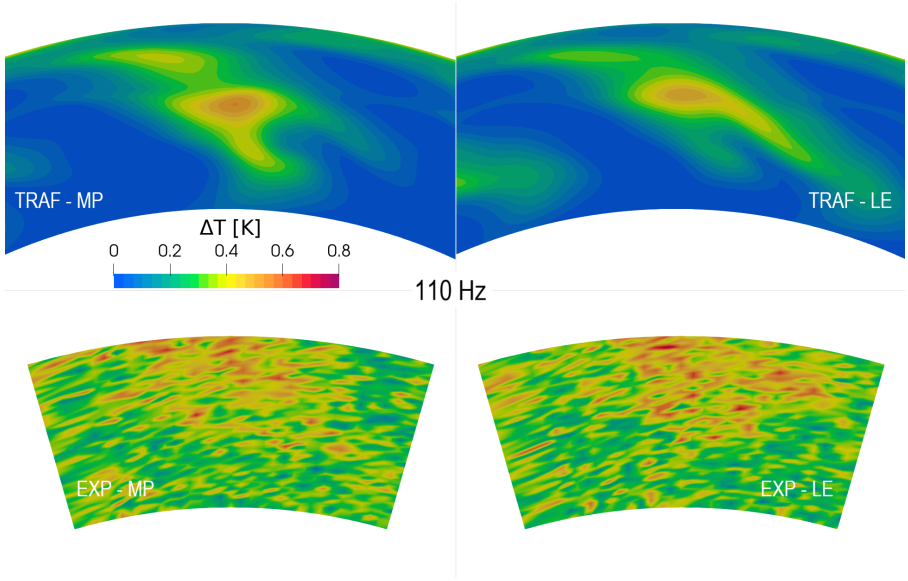

(a) Num-exp comparison for CCW swirling flow

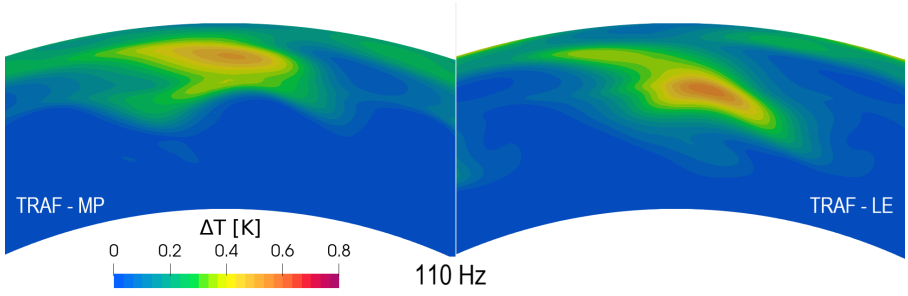

(b) Num-exp comparison for CW swirling flow

Fig. 15: 110 Hz: amplitude of EW temperature oscillations at the rotor exit (plane T3)

Effect of swirling EW on rotor secondary flows

The effect of the EW on the rotor secondary flows has been only numerically addressed. The “clean” case is firstly discussed to underline the main vortical structure depicted in Fig.16a. The hub and tip passage vortexes are clearly visible near the blade suction side. In details, the hub passage vortex (HPV) moves up to the blade mid-span and is highlighted by the wide area with positive vorticity, while the tip passage vortex (TPV) is located between the hub passage vortex and the tip clearence vortex (TCV) shown by blue and red areas respectively in the upper part of the channel.

The effect on the secondary flows of the rotors is now due only to the temperature gradient introduced

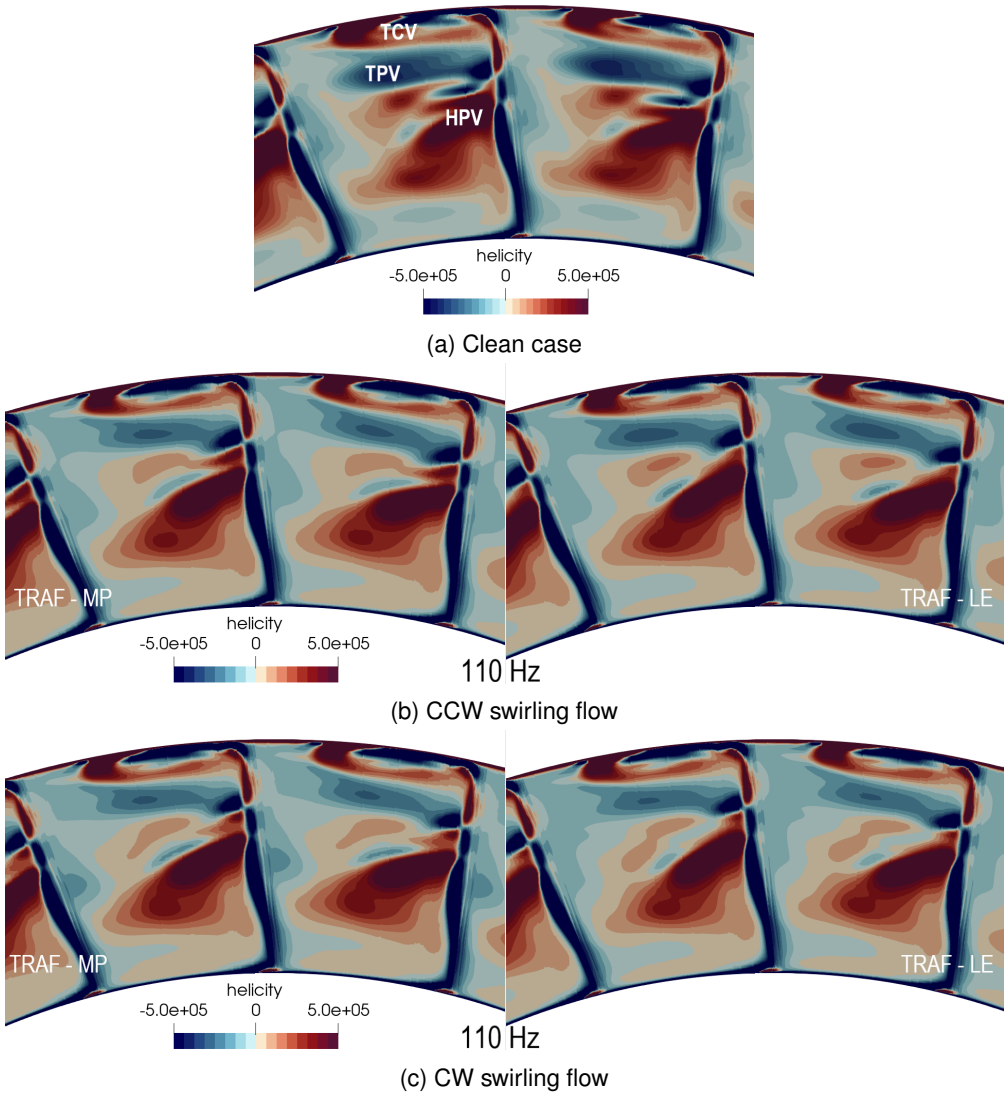

(a) Clean case

(b) CCW swirling flow

(c) CW swirling flow

Fig. 16: 110 Hz: helicity contours at the rotor exit (plane T3) from numerical simulations

by the EW presence (as already pointed out in [14]), and is located around mid-span where the two passage vortexes are close. Both CCW and CW swirl directions at MP and LE positions reveal only small secondary flow modifications, where the core of the entropy fluctuation is located.

Entropy noise generation

The post-processing strategy, proficiently employed for the isolation of the EW envelope, can be further used to extract the entropy noise emissions at the stage inlet and outlet [22]. It has already been demonstrated that swirling EWs have a detrimental effect on stage efficiency and can lead to thermal issues, but they are also responsible for indirect noise generation. As stated in the introduction, the indirect combustion noise (or entropy noise) is generated when temperature fluctuations are accelerated in a nozzle as a HP stator vane. The acceleration of the entropy spot which transports a non-acoustic density fluctuation, generates a fluctuating force which acts as an acoustic “dipole” thus generating source of the indirect noise that propagates upstream and downstream.

Since the EW fluctuations have a low frequency, all the possible spinning lobes composing the overall entropy noise signature are basically cut-off, except for the circumferential order equal to zero. By extracting this acoustic mode at the domain extremities the outgoing indirect emissions can be evaluated. At the domain inlet, the outgoing wave interacts with the combustor and may be reflected back to the stage further increasing the indirect noise emitted; while the acoustic wave exiting the stage at the outlet propagates down towards the exhaust and directly contribute to the overall noise signature. The acoustic extraction method

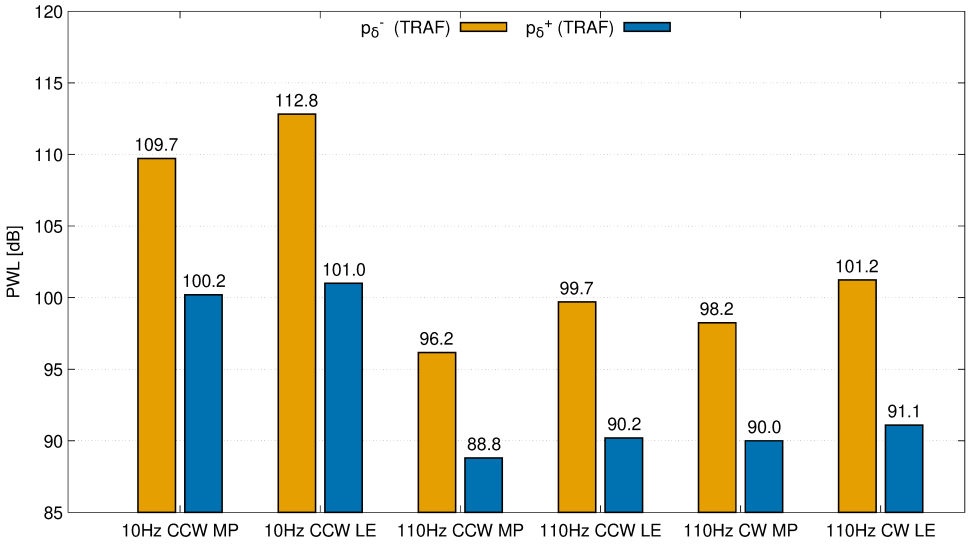

Fig. 17: Entropy noise emission at the stage inlet (plane T1)

is based on the flow characteristic following the approach proposed by Giles [33] allowing the separation of upstream and downstream components. Figure 17 collects the indirect acoustic emission in term of sound power level (PWL) at the domain inlet. The p_δ^- and p_δ^+ are the upstream running and downstream running pressure waves respectively. At the stage inlet, the outgoing waves are the p_δ^-, while the downstream running ones are spurious reflections generated at the domain inlet. As can be seen, the latter are lower than 6 dB with respect to the upstream running components thus ensuring a good non-reflectiveness of the inlet domain treated by Giles non-reflecting boundary conditions [33]. With the same concept, Fig. 18 reports the pair of acoustic waves at the stage outlet. This time, the outgoing waves are the downstream running components, while the upstream running ones are again spurious reflections that are kept low by the buffer zone treatment [31]. Indeed they are lower than 6 dB with respect to the p_δ^+. This confirms that spurious reflections do not pollute the inner fluctuating field.

Looking at the two histograms, it is clear that the 10 Hz CCW EW fluctuations generate the higher acoustic emissions as the EW spot shows the highest ΔT. At the stage inlet, the 10 Hz CCW LE case reveals the loudest emission (see Fig. 17): this is due to the fact that the highest temperature fluctuation impinges the leading edge and undergoes the highest acceleration on the front part of the stator directing the entropy noise emission towards the stage inlet. On the contrary, the 10 Hz CCW MP spot is mostly accelerated in the rear part of the stator channel, and thus the indirect noise is directed downstream, causing to the highest emission at the stages outlet (see Fig. 18). The 110 Hz CCW cases show outgoing

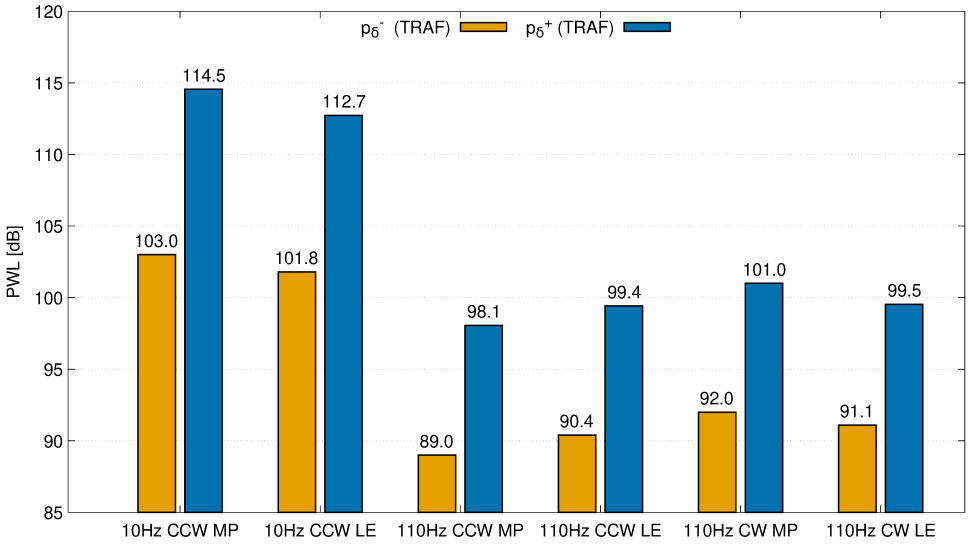

Fig. 18: Entropy noise emission at the stage outlet (plane T3)

emissions more than 10 dB lower than the 10 Hz cases: this is due to the fact that the EW spot is highly reduced by the mixing process carrying on a low energetic content before being accelerated. Finally, the 110 Hz CW case reveals slightly higher emissions with respect to the CCW case because the EW spot remains more coherent in the stator vane (see Fig. 10b) and higher ΔT value are present where the spot is accelerated.

CONCLUSIONS

The impact of swirling entropy waves imposed at the inlet of a HP turbine stage is described in this study, and an accurate comparison between experimental data and numerical results is presented and discussed.

First an analysis on the impact on the stage efficiency of the different injection frequencies, clocking positions between the injector and the stator vane, swirling direction is proposed to assess the overall results: experiments and CFD showed a very good agreement in all the cases. Compared with the “clean” case, the injection of the disturbances always reduces the efficiency with different rates depending on the position, frequency, and swirl direction. In general, the 10 Hz frequency has a larger impact compared to the 110 Hz frequency, this is because it is associated with a higher temperature fluctuation at the inlet that persists downstream of the stator and impacts on the rotor performance.

The change of the swirl direction modifies the interaction with the secondary flows of the stator row. The lowest interaction is found for the clockwise rotation (CW) since in this case the EW swirl is opposite to the tip passage vortex. In fact, since the EW is injected close to mid-span and the tip passage vortex formation starts close to the casing, the two vortical structures persist separately and do not merge in the interaction region, as it would happen in the co-rotating case (CCW).

The injection position, vane- or passage-aligned, influences the interaction with the blade and for this reason, impacts the swirling and the entropy wave magnitude. In the vane-aligned counter-rotating case, the temperature level downstream of the stator is higher compared to the passage-aligned case, this latter being more diffused in the transport inside the vane.

The secondary flow system of the rotor is also slightly affected by the swirling entropy waves due to the presence of the temperature gradients generated by the EW envelope that is located in the mid-span region where the higher modification of secondary flow structure is observed.

Finally, thanks to the post-processing capabilities, the indirect noise emissions due to the acceleration of the EW spot within the stage have been assessed. The 10 Hz cases showed the loudest emissions, and

it has been noted that the PWL extracted at the stage inlet and outlet depends on the stator channel region where the EW acceleration occurs.

All these conclusions can be used from a design point of view to reduce the detrimental effect of combustor distortions on the stage efficiency, thermal implication and entropy noise generation.

NOMENCLATURE

p_δ^- , p_δ^+	up/downstream running acoustic waves
T	temperature

Acronyms:

BPF	Blade Passing Frequency
CCW	Counterclockwise
CW	Clockwise
EWF	Entropy Wave Frequency
EWG	Entropy Wave Generator
EW	Entropy Wave
FRAPP	Fast Response Aerodynamic Pressure Probe
HS	Hot Streak
LE	Leading Edge (EW injector position)
MP	Mid Pitch (EW injector position)
PWL	Power Watt Level

REFERENCES

[1] Sharma, O., Pickett, G., and Ni, R., 1992. "Assessment of unsteady flow in turbines". *ASME J. Turbomach.,* **114**, pp. 79–90.

[2] Butler, T., Sharma, O., Joslyn, H., and Dring, R., 1989. "Redistribution of an inlet temperature distortion in an axial flow turbine stage". *J. Propul. Power,* **5**, pp. 64–71.

[3] Dorney, D., and Sondak, D., 2000. "Effects of tip clearance on hot streak migration in a high subsonic single stage turbine". *ASME J. Turbomach.,* **122**, pp. 613–620.

[4] An, B., Liu, J., and Jiang, H., 2009. "Numerical investigation on unsteady effects of hot streak on flow and heat transfer in turbine stage". *ASME J. Turbomach.,* **131**. 031015.

[5] Jacobi, S., Mazzoni, C., Chana, K., and Rosic, B., 2017. "Investigation of unsteady flow phenomena in the first vane caused by the combustor flow with swirl". *ASME J. Turbomach.,* **139**. 041006.

[6] Morgans, A. S., and Durán, I., 2016. "Entropy noise: A review of theory, progress and challenges". *International Journal of Spray and Combustion Dynamics,* **8**, pp. 285 – 298.

[7] Dowling, A. P., and Mahmoudi, Y., 2015. "Combustion noise". *Proceedings of the Combustion Institute,* **35**(1), pp. 65–100.

[8] Giles, M., and Saxer, A., 1994. "Predictions of three-dimensional steady and unsteady inviscid transonic stator/rotor interaction with inlet radial temperature nonuniformity". *ASME J. Turbomach.,* **116**, pp. 347–357.

[9] Ong, J., and Miller, R., 2012. "Hot streak and vane coolant migration in a downstream rotor". *ASME J. Turbomach.,* **134**. 051002.

[10] Koupper, C., Bonneau, G., and Gicquel, L., 2016. "Large eddy simulation of the combustor turbine interface: Study of the potential and clocking effects". In IGTI ASME Turbo Expo. ASME paper GT2016-56443.

[11] Gaetani, P., Persico, G., Pinelli, L., Marconcini, M., and Pacciani, R., 2020. "Computational and Experimental Study of Hot Streak Transport Within the First Stage of a Gas Turbine". *Journal of Turbomachinery,* **142**(8), 07. 081002.

[12] Giusti, A., Worth, N. A., Mastorakos, E., and Dowling, A. P., 2017. "Experimental and numerical investigation into the propagation of entropy waves". *AIAA Journal,* **55**(2), pp. 446–458.

[13] Gaetani, P., and Persico, G., 2018. "Transport of entropy waves within a hp turbine stage". *Journal of Turbomachinery,* **141**, 12.

[14] Pinelli, L., Marconcini, M., Pacciani, R., Gaetani, P., and Persico, G., 2021. "Computational and Experimental Study of the Unsteady Convection of Entropy Waves Within a High-Pressure Turbine Stage". *Journal of Turbomachinery,* **143**(9), 05. 091011.

[15] Kaji, S., and Okazaki, T., 1970. "Generation of sound by rotor–stator interation". *Journal of Sound and Vibration,* **13**(3), pp. 281–307.

[16] Rahim, A., and He, L., 2015. "Rotor Blade Heat Transfer of High Pressure Turbine Stage Under Inlet Hot-Streak and Swirl". *Journal of Engineering for Gas Turbines and Power,* **137**(6), 06. 062601.

[17] Adams, M. G., Povey, T., Hall, B. F., Cardwell, D. N., Chana, K. S., and Beard, P. F., 2020. "Commissioning of a Combined Hot-Streak and Swirl Profile Generator in a Transonic Turbine Test Facility". *Journal of Engineering for Gas Turbines and Power,* **142**(3), 01. 031008.

[18] Adams, M. G., Beard, P. F., Stokes, M. R., Wallin, F., Chana, K. S., and Povey, T., 2021. "Effect of a Combined Hot-Streak and Swirl Profile on Cooled 1.5-Stage Turbine Aerodynamics: An Experimental and Computational Study". *Journal of Turbomachinery,* **143**(2), 02. 021011.

[19] Notaristefano, A., and Gaetani, P., 2020. "Design and commissioning of a combustor simulator combining swirl and entropy wave generation". *International Journal of Turbomachinery, Propulsion and Power,* **5**(4).

[20] Notaristefano, A., and Gaetani, P., 2021. "Impact of Swirling Entropy Waves on a High Pressure Turbine". *Journal of Turbomachinery,* **144**(3), 10. 031010.

[21] Bicchi, M., Pinelli, L., Marconcini, M., Gaetani, P., and Persico, G., 2019. "Numerical study of a high-pressure turbine stage with inlet distortions". *AIP Conference Proceedings,* **2191**(020020), 12.

[22] Pinelli, L., Marconcini, M., Pacciani, R., Bake, F., Knobloch, K., Gaetani, P., and Persico, G., 2022. "Effect of clocking on entropy noise generation within an aeronautical high pressure turbine stage". *Journal of Sound and Vibration,* **529**, p. 116900.

[23] Notaristefano, A., Gaetani, P., Dossena, V., and Fusetti, A., 2021. "Uncertainty Evaluation on Multi-Hole Aerodynamic Pressure Probes". *Journal of Turbomachinery,* **143**(9), 05. 091001.

[24] Gaetani, P., Persico, G., and Guardone, A., 2005. "Design and analysis of new concept fast-response pressure probes". *Meas. Sci.Technol.,* **16**. 1741–1.

[25] Arnone, A., 1994. "Viscous analysis of three-dimensional rotor flow using a multigrid method". *Journal of Turbomachinery,* **116**, pp. 435–445.

[26] Pacciani, R., Marconcini, M., and Arnone, A., 2019. "Comparison of the AUSM+-up and other advection schemes for turbomachinery applications". *Shock Waves,* **29**, 01.

[27] Pacciani, R., Marconcini, M., Bertini, F., Rosa Taddei, S., Spano, E., Zhao, Y., Akolekar, H. D., Sandberg, R. D., and Arnone, A., 2021. "Assessment of machine-learned turbulence models trained for improved wake-mixing in low-pressure turbine flows". *Energies,* **14**(24).

[28] Pinelli, L., Poli, F., Di Grazia, E., Arnone, A., and Torzo, D., 2013. "A comprehensive numerical study of tone noise emissions in a multistage cold flow rig". In 19^{th} AIAA/CEAS Aeroacoustic Conference. AIAA paper 2013-2104, 27-29 May, Berlin, Germany.

[29] Pinelli, L., Lori, F., Marconcini, M., Pacciani, R., and Arnone, A., 2021. "Validation of a modal work approach for forced response analysis of bladed disks". *Applied Sciences,* **11**(12).

[30] Pinelli, L., Amedei, A., Meli, E., Vanti, F., Romani, B., Benvenuti, G., Fabbrini, M., Morganti, N., Rindi, A., and Arnone, A., 2021. "Innovative Design, Structural Optimization, and Additive Manufacturing of

New-Generation Turbine Blades". *Journal of Turbomachinery,* **144**(1), 09. 011006.

[31] Burberi, C., Ghignoni, E., Pinelli, L., and Marconcini, M., 2018. "Validation of an URANS approach for direct and indirect noise assessment in a high pressure turbine stage". *Energy Procedia,* **148**, pp. 130–137. ATI 2018 - 73rd Conference of the Italian Thermal Machines Engineering Association.

[32] Giovannini, M., Marconcini, M., Arnone, A., and Bertini, F., 2014. "Evaluation of Unsteady CFD Models Applied to the Analysis of a Transonic High-Pressure Turbine Stage". *P. I. Mech. Eng. A-J. Pow.,* **228**(7), pp. 813–824.

[33] Giles, M. B., 1990. "Nonreflecting boundary conditions for euler equation calculations". *AIAA Journal,* **28**(12), pp. 2050–2058.